# Designing and Development of Hyperspectral Camera to Hidden Targets Detection

Hamid Reza Bakhtiari [a*], Abolfazl Chaman Motlagh[b], Abbas Bashiri [c]

[a] *M.Eng student of Electronic, Microelectronic and Nanoelectronic Devices, Department of Information and Communication Technology, Imam Hossein University, Tehran, Iran*

[b] *Assistant Professor of Electronic, Department of Information and Communication Technology, Imam Hossein University, Tehran, Iran*

*Achaman@ihu.ac.ir.*

[c] *Instructor of Electronic, Department of Information and Communication Technology, Imam Hossein University, Tehran, Iran*
*kpbashiri@ihu.ac.ir*

## Abstract

One of the major strengths resulting from hyperspectral imaging is target detection, specifically subpixel detection, which is generally carried out without full knowledge of the targets to be detected. The aim of this study is to design and develop a hyperspectral camera and then testing its results in hidden target detection domain. For this purpose, a coin was hidden under a cloth in a laboratory environment and then was take hyperspectral imaging of the hidden target. Initially, the images were labeled in terms of wavelength and band and geometric corrections and used for final processing. In order to detect image anomalies, the RX algorithm was used locally to identify pixels that are spectrally different from other pixels. To identify hidden target material, spectra of extracted as anomalies pixels were extracted and by using of the spectral library, hidden target material was identified. The accuracy of the extracted spectra was evaluated by the spectral angle, ACE , Likelihood and FP  correlation methods and the results showed high accuracy of the target material identification process.

*Keywords:* hyperspectral camera, hidden target detection, anomaly, RX algorithm, accuracy assessment.

* Corresponding author. Tel: +98-9137969114.
*Email address: g9612417365@ihu.ac.ir.*

## 1. Introduction

Hyperspectral imagers enable the collection of a series of contiguous, very narrow spectral bands, providing a near-continuous spectrum of an object, commonly referred to as the spectral signature (Alejandra et al., 2019 & Stuart et al., 2019). The spectral signature of a material in the Vis-NIR spectral domain is characterized by its general forms, the intensity of its reflectance, and specific absorption bands (Gomez & Lagacherie, 2016). The hyperspectral camera can be more sensitive and capable to transfer this information into qualitative or quantitative data (Baur et al., 2019). Hyperspectral system initially samples the light, it passes through a slit which disperse it (Mahajan & Kamalapur., 2016). Pushbroom imaging systems are based on using slit aperture to scan the image in a line by line fashion (Xu et al., 2018), which is faster and more efficient, since it requires scanning across only one spatial dimension of the image (Abdo et al., 2019 & Huber et al., 2018). Target detection is one of the most important applications of hyperspectral images (Zhang et al., 2019), that extracted by using many algorithms in the field of hyperspectral signature analysis (Bitar et al., 2019).

Gutierrez et al. (2019), proposed a custom scanning hyperspectral imaging system for biomedical applications, modeling, benchmarking, and specification. This article described a rotating mirror scanning hyperspectral imaging device, its multiparametric model, as well as design and calibration protocols. This study used general explanations to develop the imaging system and imaging modality.

Reza et al. (2019), proposed a simplified methodology to enable accurate and reliable characterization of a commercial hyperspectral camera and spectral calibration of its output data. A calibration coefficient determined for the spectral acquisition range (400- 1000 nm), and native resolution (2.7 nm), to transfer raw hyperspectral data into spectral radiance in the SL unit. Different spectral resolutions were also tested in this study to minimize data size and maintain spectral accuracy. The spectral were validated under LED fluorescent.

Vemuri et al. (2019), proposed a generic framework for quantitative and application- specific performance assessment of HIS camera and optical subsystem without the need for any physical setup. This framework quantifies the performance of the given camera configuration using a large amount of simulated data and user-defined metrics. The advantage of being able to test the desired configuration without the need for purchasing expensive components may save system engineers valuable resources.

Yang et al. (2019), proposed a novel anomaly detection algorithm via dictionary construction based low rand representation and adaptive weighting. The results of this study showed that he anomaly pixel is more easily distinguished from the background. Accuracy assessments demonstrate the superiority of our proposed method over other AD detectors.

In this study, a VNIR[1] hyperspectral camera was designed and developed and was tested in the lab situation for hidden target detection.

---

1. Visible-NIR
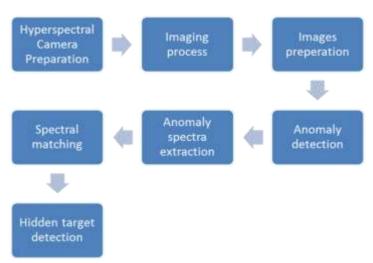
## 2. Material and Methods



**Figure1.** Flowchart of research phases

2.1. Hyperspectral Camera

Pushbroom HSI[1] has been used in many areas from air to land. However, its inherent operational drawback of the bulky slit leads to a limited FOV[2] and high energy consumption (Dong et al., 2019). Hyperspectral pushbroom imaging system usually consists of five major parts: illumination unit, spectrograph, camera (detector), translation stage, and image processing unit. *Figure (2)*, shows a schematic of hyperspectral data acquisition.
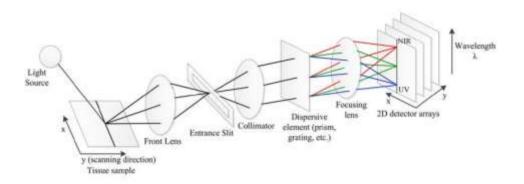


**Figure2.** Schematic diagram of a pushbroom hyperspectral imaging system (Lu & Fei, 2014)

A tungsten lamp has been used as a light source of the constructed hyperspectral imager. The advantage of the used tungsten lamp is its wide spectral range starting at approximately 420 nm and continues to more than 1000 nm. At the beginning of spectrograph, an objective lens (with a focal length of 75 mm) was located and then, a slit respectively with 7mm and $200\mu$m length and width was embedded before the collimating lens. The diffraction grating was applied as a dispersive element and a 25mm focal length

————

1. hyperspectral imaging
2. field of view

focusing lens was used at the end before the CCD[1] detector. A Stepper Motor-based translation stage was used to scan the target completely, and finally, a computer was processed acquired images.

The hyperspectral imaging system is capable of imaging objects in the spectral range of 420 to 900 nm in 480 bands and having a spectral resolution of 1 nm. NI Labview software also was used to control and process all imaging steps.

2.2. Image Processing

Usually, a hyperspectral image contains thousands of spectral pixels. The image files generated are large and multidimensional, which makes visual interpretation difficult at best. Many digital image processing techniques are capable of analyzing multidimensional images (Nagadi & Liu., 2010).

Generally, these are adequate and relevant for hyperspectral image processing. Several classic target detection algorithms for multispectral and hyperspectral data have been proposed, such as ACE, CEM[2], GLRT[3], ASD[4], OSP[5], SAM[6] and etc. (Liu & Li., 2018). The processing methods developed for environmental classification are not applicable to target detection for two reasons: First, the number of targets in a scene is typically too small to support the estimation of statistical properties of the target class from the scene. Second, depending upon the spatial resolution of the sensors, targets of interest may not be clearly resolved, and hence they appear in only a few pixels or even a single pixel (Manolakis et al., 2013).

2.2.1. Anomaly Detection

Anomaly detection involves modeling the background and using the difference between the pixels and the background to detect anomalous pixels (Tan et al., 2019). Many algorithms have been developed for anomaly detection over the years and can be roughly categorized into two classes, second-order statistics methods and high order statistics methods. The detector in the first class can be considered as either mahalanobis distance-based filters which are variants of algorithm, refer as RX[7] detector (RXD), or matched filter based detectors derived from R-RXD (Chang, 2016 & Basora et al., 2019).

2.2.1.1. RX Anomaly Detection Algorithm

The RX algorithm includes global and local RX. Since the local RX algorithm is more effective in detecting small targets. The local RX algorithm is usually used. The algorithm is assumed that the background distribution satisfied the local Gaussian distribution model, thereby calculating the mean and covariance matrix of the background pixels. Under the background model, the double window sliding method is used for detection, as shown in *figure (3):*

————

1. Charge Coupled Device
2 constrained energy minimization
3 generalized likelihood ratio test
4 Autism spectrum disorder
5 Orthogonal subspace projection
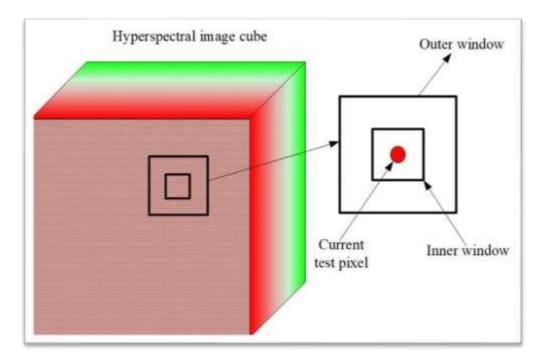6 Spectral Angle Mapper
**7** Reed-Xiaoli

**Figure3.** Hyperspectral anomaly target local detection model (Zhang et al., 2019)

The specific implementation process of RX algorithm is as follows: define $X_R$ as a background matrix of L x N, L is the number of bands, N is the number of pixels, and the detected pixels $X_i$ can be expressed as:

$$X_i = [x_{i1}, x_{i2}, x_{i3}, ..., x_{iL}] \tag{1}$$

The binary hypothesis test of the RX algorithm can be expressed as:

$$\begin{cases} H_0 : r = n \\ H_1 : r = a * s + n \end{cases} \tag{2}$$

Where r is the spectral information of the measured pixel, n is the background spectral information, a is the signal abundance, and s is the target spectral information. When a=0, the assumption $H_0$ is established as the background pixel; When a>0 the assumption $H_1$ is established as a target pixel. The discriminant of the RX algorithm based on GLRT is:

$$RX(r) = (r - \mu)^T K^{-1}(r - \mu) \begin{vmatrix} \geq \eta, H_1 \\ < \eta, H_0 \end{vmatrix} \tag{3}$$

Where $\eta$ is the discriminant threshold, the set value is related to the false alarm rate and the signal to noise ratio; $\mu$ and K are the background mean and the covariance matrix, respectively expressed as:

$$\mu = \frac{1}{n} \sum_{i=1}^{N} X_i$$

$$K = \frac{1}{n} \sum_{i=1}^{N} (x_i - \mu)(x_i - \mu)^T \tag{4}$$

The RX algorithm has several shortcomings: First, the background hypothesis is a local Gaussian distribution model. However, the distribution of features, in reality, is complex and variable. In many cases, the distribution of hyperspectral image data cannot be fully described. Second, the RX algorithm cannot fully utilize high order data of hyperspectral ignoring the nonlinear data of the image, resulting in poor detection performance (Zhang et al., 2019).

## 3. Results and discussion

In order to implement the algorithms, firstly, an image of a coin hidden beneath the cloth was captured by use of designed hyperspectral camera. *Figure (4)*, shows the captured image.
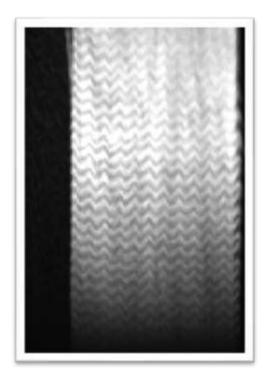


**Figure4.** Image of coin beneath cloth captured by hyperspectral camera.

RX algorithm was used to detect image anomalies and coin extraction. Pixels from the image known as anomalies were extracted and selected for material identification. *Figure(5)*, shows anomaly pixels.
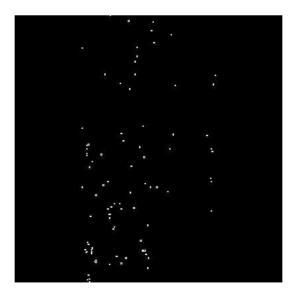


**Figure5.** Anomaly pixels of image

Selected pixels, was tested using a pre-prepared spectral library to identify the most similar spectrum to

the anomaly pixels spectral. Based on the spectral library, the extracted spectrum was a combination of copper metal and aluminum metal spectra. *Figure(6)*, shows the spectra of material identification.
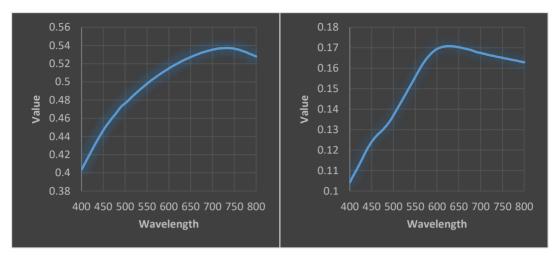


*Figure6*. Spectral of Aluminum metal (left) and copper metal (right)

Spectral angle, ACE, Likelihood, and FP correlation methods were used to evaluate the accuracy of the extracted spectra. Table (1), shows the accuracy assessment of spectrals.

**Table1.** Accuracy Assessment of Extracted Spectral.

|  | **Spectral Angle** | **ACE** | **Likelihood** | **FP correlation** |
|---|---|---|---|---|
| **Copper metal** | 0.06 | 0.85 | 0.88 | 0.84 |
| **Aluminum metal** | 0.09 | 0.83 | 0.81 | 0.88 |

**Spectral Angle:** Indicates the separation of reference and extracted spectra. Smaller spectral angles are better matches.

**ACE:** ACE measures if a reference spectrum is a good match for the spectrum in the selected image. ACE values range from -1 to 1 with scores close to 1 indicating a best match.

**Likelihood:** Likelihood measures how good a spectrum is in comparison to the other spectrum in the library. If the likelihood for spectra A is twice that of spectra B, then the probability of spectra A is twice that of the probability for B. The likelihoods will all sum to 1.

**FP correlation:** Full Pixel Correlation measures how good the pixel spectrum matches each library spectrum. Correlation values range from -1 to 1 with scores close to 1 indicating the best match.

In this study, images of the designed hyper-spectral camera were used to identify hidden targets. Identifying the hidden target beneath the cloth required the precision processing methods used for this purpose. The use of anomaly detection methods led to the whole area under study for spectral anomalies searches. The under-purpose spectral library helped us to classify the detected anomalies accordingly. Using this type of verification resources makes it possible to identify targets with high accuracy.

The results of this study is in consistency with (Dong et al., 2018 & Gao et al., 2015). In comparison to (Wolfgange et al., 2015), that only used shape information of targets, this study used spectral and texture information together for hidden target detection. (Puttonen et al., 2015), used Hyperspectral and Lidar data integration for artificial target detection. In comparison of this study, we only used Hyperspectral data and don't integrate with other data set. Designing a hyperspectral camera, using hidden targets, identifying hidden target material and spectral library development, are the innovations and advantages of this study depending on those of the present study.

## 4. Conclusions

In this study, firstly, a hyperspectral camera was designed that has a very high spectral resolution and is suitable for multiple studies. To evaluate the camera's performance, a hidden target was used and then imaged. The use of the RX anomaly detection algorithm gave a very good performance due to its performance in both local and global domains. Because the hidden target had very few fingerprints in the cloth area, the local method was used to detect the target anomaly, while identifying changes in target and background spectra more thoroughly, target identification is performed with high accuracy. Target material identification was one of the limitations of similar work, with the use of a pre-made spectral library to identify target material with high accuracy. In the following, it is recommended to identify hidden targets using different thicknesses of clothes.

## References

Abdo, M., Badilita, V., & Korvink, J. (2019). Spatial scanning hyperspectral imaging combining a rotating slit with dove prism. Optic express, (27), 20290- 20304.

Alejandra, M., Barreto, P., Johansen, K., Angel, Y., & McCabe, M. (2019). Radiometric assessment of a UAV-based push broom hyperspectral camera. Sensors, (19), 1-22.

Basora, L., Olive, X., & Dubot, Th. (2019). Recent advances in anomaly detection methods applied to aviation. Aerospace, (6), 1-27.

Baur, J, R., Brunis, A., Hardeberg, J, Y., & Verdaasdonk, R, M. (2019). A spectral filter array camera for clinical monitoring and diagnosis: proof of concept for skin oxygenation imaging. Imaging, (5), 1-23.

Bitar, A. W., Ovarlez, J. P., Cheong, L. F., & Chehab, A. (2019). Automatic target detection for sparse hyperspectral images. arXiv preprint arXiv:1904.09030.

Chang, C, I. (2016). Real time progressive hyperspectral image processing. Springer, New York, USA.

Dong, X., Xiao, X., Pan, Y., Wang, G., & Yu, Y. (2019). DMD-based hyperspectral systems with tunable spatial and spectral resolution. Optics express, (27), 16995-17006.

Dong, Y., Du, B., Zhang, L., & Hu, X. (2018). Hyperspectral target detection via adaptive information – Theoretic metric learning with local constraint. Remote sensing, (10).

Gutierrez, J, A., Pardo, A., Real, E., Higuera, J, M., & Conde, O, M. (2019). Custom scanning hyperspectral imaging system for biomedical applications: modeling, benchmarking and specification. Sensors, (19), 1692.

Gao, L., Yang, B., Du, Q., & Zhang, B. (2015). Adjusted spectral matched filter for target detection in hyperspectral imagery. Remote sensing, (7).

Gomez, C., & Lagacherie, Ph. (2016). Mapping of primary soil properties using optical visible and near infrared remote sensing. Land surface remote sensing in agriculture and forest, 1-35.

Huber, G., Sang, B., Erhard, M., Staton, G., Honold, H, P., Schmitt, H., Zauner, Ch., Sornig, M., & Fischer, S. (2018). An all silicon high precision double slit device for hyperspectral imager EnMap. SPIE, (2018).

Lu, G., & Fei, B. (2014). Medical hyperspectral imaging: a review. Journal of biomedical optics, (19), 1-23.

Liu, D., & Li, J. (2018). Spectral-spatial target detection based on data field modeling for hyperspectral data. Chines journal of aeronautics, (31), 795-805.

Manolakis, D., MArden, D., & Shaw, G, A. (2013). Hyperspectral image processing for automatic target detection application. Lincoln laboratory journal, (14), 79-116.

Mahajan, M, P., & Kamalapur, S, M. (2016). Hyperspectral imaging. Asian journal of computer science engineering, (2), 6-10.

Nagadi, M, O., & Liu, L. (2010). Hyperspectral imaging for food quality analysis and control. Elsevier.

Puttonen, E., Hakala, T., Nevalanien, O., Kaasalanien, S., Krooks, A., Karjalanien, M., & Anttila, K.(2015). Artificial target detection with a hyperspectral lidar over 26-h measurement. SPIE, (54), 1-15.

Reza, A., Jost, S., Dubail, M., & Dumortier, D. (2019). Simplified hyperspectral camera calibration for accurate radiometric measurement. 29th CIE session, Washington, USA.

Stuart, M., McGonigle, A., & Willmot, R. (2019). Hyperspectral Imaging in Environmental Monitoring: A Review of Recent Developments and Technological Advances in Compact Field Deployable Systems. Sensors, 19.

Tan, K., Hou, Z., Wu, F., Du, Q., & Chen, Y. (2019). Anomaly detection for hyperspectral imagery based on

the regularized subspace method and collaborative representation. Remote sensing, (11), 1-22.

Vemuri, A, S., Wirkert, S., & Hein, L, M. (2019). Hyperspectral camera selection for interventional health-care. ArXav, 1-13.

Wolfgange, G., Jonas, B., Hendrick, Sc., Wolfgange, M., Jorg, W., Peter, W., Roland, O., & Mathias, K.(2015). Assessment of target detection limits in hyperspectral images. Zurich open repository and archive, 9653, 1-10.

Xu, Y., Chen, J., Liyang, L., & Kelly, K, F. (2018). Compressive hyperspectral microscopy of nanomaterial's. RAPID conference, Miramar beach, USA.

Yang, Y., Zhang, J., Song, Sh., & Liu, D. (2019). Hyperspectral anomaly detection via dictionary construction based low rank representation and adaptive weighting. Remote sensing, (11), 1-26.

Zhang, Y., Hua, W., Huang, F., Wang, Q., & Suo, W. (2019). Research status of hyperspectral anomaly target detection. ICAITA, 1-6.